CLIMATOLOGY

Amplified seasonality in western Europe in a warmer world

Niels J. de Winter[1,2]*, Julia Tindall[3], Andrew L. A. Johnson[4], Barbara Goudsmit-Harzevoort[5,6], Nina Wichern[7], Pim Kaskes[2,8], Philippe Claeys[2], Fynn Huygen[9], Sonja van Leeuwen[5], Brett Metcalfe[1,10], Pepijn Bakker[1], Stijn Goolaerts[11], Frank Wesselingh[6,12], Martin Ziegler[6]

Documenting the seasonal temperature cycle constitutes an essential step toward mitigating risks associated with extreme weather events in a future warmer world. The mid-Piacenzian Warm Period (mPWP), 3.3 to 3.0 million years ago, featured global temperatures approximately 3°C above preindustrial levels. It represents an ideal period for directed paleoclimate reconstructions equivalent to model projections for 2100 under moderate Shared Socioeconomic Pathway SSP2-4.5. Here, seasonal clumped isotope analyses of fossil mollusk shells from the North Sea are presented to test Pliocene Model Intercomparison Project 2 outcomes. Joint data and model evidence reveals enhanced summer warming (+4.3° ± 1.0°C) compared to winter (+2.5° ± 1.5°C) during the mPWP, equivalent to SSP2-4.5 outcomes for future climate. We show that Arctic amplification of global warming weakens mid-latitude summer circulation while intensifying seasonal contrast in temperature and precipitation, leading to an increased risk of summer heat waves and other extreme weather events in Europe's future.

INTRODUCTION

The mid-Piacenzian Warm Period (mPWP) represents an interval with global mean surface temperature estimated on average 3.2°C (1.7° to 5.2°C) higher than in preindustrial modern times due predominantly to elevated atmospheric CO_2 concentrations [~400 parts per million by volume (ppmV)] (*1*–*3*). Temperatures during this period closely resemble the global mean surface temperature projected for the year 2100 following the Shared Socioeconomic Pathway (SSP) 2-4.5 (*4*–*7*), the SSP scenario most likely to be realized given current global climate policy (*8*). The Pliocene Model Intercomparison Project 2 (PlioMIP2) consortium has targeted the mPWP using an ensemble of General Circulation Models (*9*). This allows a detailed data-model comparison, which is essential for assessing the performance of climate models simulating climate scenarios with higher temperatures than represented in instrumental records, similar to conditions that will most likely define future climate on Earth (*2*, *5*).

One region under extreme threat in a global warming scenario is the Arctic region, which is anticipated to warm up two to four times faster than the global average, a phenomenon called Arctic amplification (*10*). Model experiments using future CO_2 forcing scenarios imply that Arctic amplification caused by global warming of mPWP magnitude might affect the storm track–affected regions of Europe by weakening atmospheric summer circulation (*11*), significantly reducing summer cloud cover (*12*) and leading to persistently elevated summer temperatures and droughts (*13*, *14*). Taking into account these "dynamic" drivers of summer weather extremes, related to changes in atmospheric circulation, more extreme weather variability would be projected for the future than the variability expected from "thermodynamic" drivers of temperature changes alone (*14*). Given this season-specific response of weather patterns to warming, seasonal-scale reconstructions of mPWP climate are crucial to validate climate model simulations and improve our understanding of the impact of higher atmospheric greenhouse gas concentrations on European climate.

Yet, climate proxy records from pelagic sediment cores, which form the predominant means of estimating mPWP temperatures (*15*–*17*), rarely resolve seasonal-scale variability in the temperature cycle due to low temporal resolution. Furthermore, short-lived marine organisms that make up pelagic sediments preferentially grow only during specific seasons with favorable conditions. This seasonal bias places considerable uncertainty on marine climate reconstructions and data-model comparisons based on common temperature proxies, such as Mg/Ca and stable isotope ratios in foraminifera (*18*), TEX_{86} from membrane lipids in Crenarchaeota (*19*), and $U_{37}^{K'}$ based on ketones in haptophyte algae (*20*). These uncertainties probably account for the difficulty of reconciling seasonal-scale mPWP climate reconstructions and models of terrestrial seasonality (*21*).

One approach to facilitate seasonal data-model comparison is to use information from marine mollusks, which record daily- to decadal-scale variability in the chemistry of their calcium carbonate shells (*22*–*25*) and preserve this archive of high-resolution environmental variability over geological timescales (*26*–*28*). Climate reconstructions at the seasonal scale from mid-latitude shelf seas, where appropriate mollusks are common, are instrumental in assessing the impact of warming on the seasonal scale because these regions experience high seasonal temperature contrast and their ecosystems are strongly affected by climate change (*29*–*32*). Going a step further, by using the clumped isotope composition of shell carbonate, it becomes possible to reconstruct seasonal temperature changes of the water in which mollusks grow without relying on uncertain assumptions of the isotopic composition of past ocean water, leading to accurate reconstructions of past seasonality (*26*, *33*, *34*).

[1]Department of Earth Sciences, Vrije Universiteit Amsterdam, Amsterdam, Netherlands. [2]Archaeology, Environmental Changes and Geochemistry group, Vrije Universiteit Brussel, Brussels, Belgium. [3]School of Earth and Environment, University of Leeds, Leeds, UK. [4]School of Science, University of Derby, Derby, UK. [5]Department of Estuarine and Delta Systems, Royal Netherlands Institute for Sea Research, Texel, Netherlands. [6]Department of Earth Sciences, Utrecht University, Utrecht, Netherlands. [7]Institut für Geologie und Paläontologie, Universität Münster, Münster, Germany. [8]Laboratoire G-Time, Université Libre de Bruxelles, Brussels, Belgium. [9]Institut für Geowissenschaften, Universität Kiel, Kiel, Germany. [10]Laboratory of Systems and Synthetic Biology, Wageningen University & Research, Wageningen, Netherlands. [11]Directorate Earth and History of Life, Royal Belgian Institute for Natural Sciences, Brussels, Belgium. [12]Naturalis Biodiversity Center, Leiden, Netherlands.
*Corresponding author. Email: n.j.de.winter@vu.nl

We present seasonal sea surface temperature (SST) reconstructions based on clumped isotope analyses from well-preserved fossil mollusk shells originating from the Oorderen Member of the Lillo Formation (northern Belgium; see Materials and Methods). These sediments were deposited below fair-weather wave base (30 to 50 m water depth) in the southern North Sea (SNS) under warm, high sea-level conditions during and slightly after the mPWP [2.7 to 3.3 million years ago (Ma) (*35*, *36*); Fig. 1]. The shells record marine temperatures in the mPWP SNS (*37*), an important model ecosystem for temperate shelf seas worldwide (*38*). On the basis of the observation of sedimentary structures indicative of strong tidal mixing (*39*), the absence of dysoxic fauna (see Materials and Methods), and the observation of high spring temperatures (see Results; Figs. 2 and 3), it seems likely that the shells used in this study record conservative summer temperatures close to the true summer SST during the mPWP.

We directly compare our seasonal SST reconstructions with ensemble model simulations of seasonal temperature change in the mPWP SNS, previously produced by the PlioMIP2 consortium (*40*) as well as with instrumental temperature records in the region and Coupled Model Intercomparison Project Phase 6 (CMIP6) SSP2-4.5

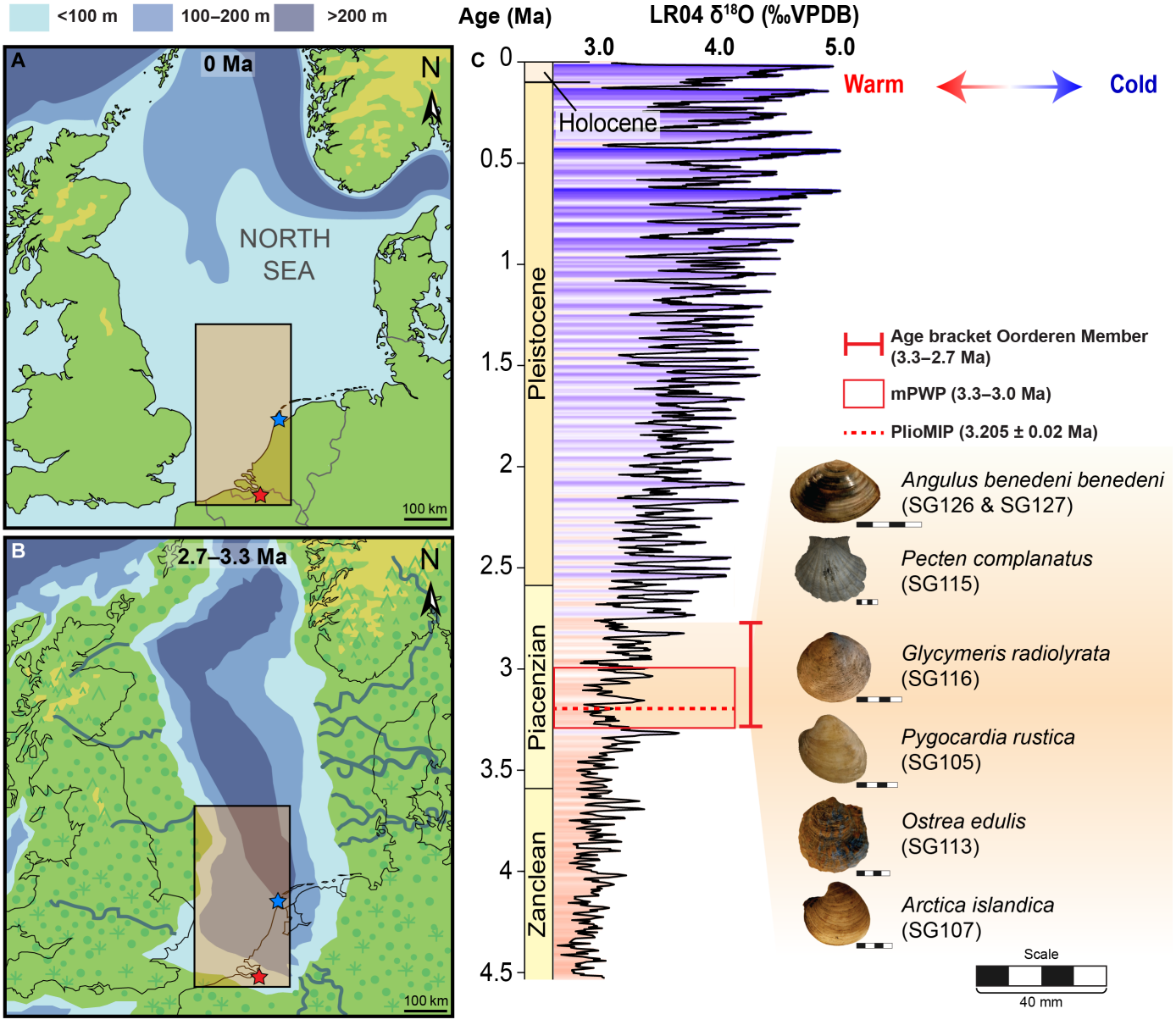

Fig. 1. Locality of the study site and long-term climate context. Maps of northwestern Europe showing the present (**A**) and estimated mPWP (**B**) [after (*35*, *37*, *67*)] SNS bathymetry. The locality of fossil shells (red star), the local modern temperature record (blue star), and the area containing the SNS data integrated from extended reconstructed SST (Extended Reconstructed SST v5), PlioMIP2, and CMIP6 models (black rectangle with orange filling; 51°N to 55°N, 2°E to 4°E; Figs. 2 and 3) are indicated. (**C**) Age bracket of the Oorderen Member (Lillo Formation) containing the mollusk specimens (*35*) (orange shaded region) relative to the mPWP (*82*) (red box) and PlioMIP2 (*1*) interval (red dashed line) and the global benthic foraminifera oxygen isotope stack (*83*) with the relative temperature change indicated. Note that mollusk specimens likely originate from highstand (i.e., warmer) periods within the age bracket (see Materials and Methods).

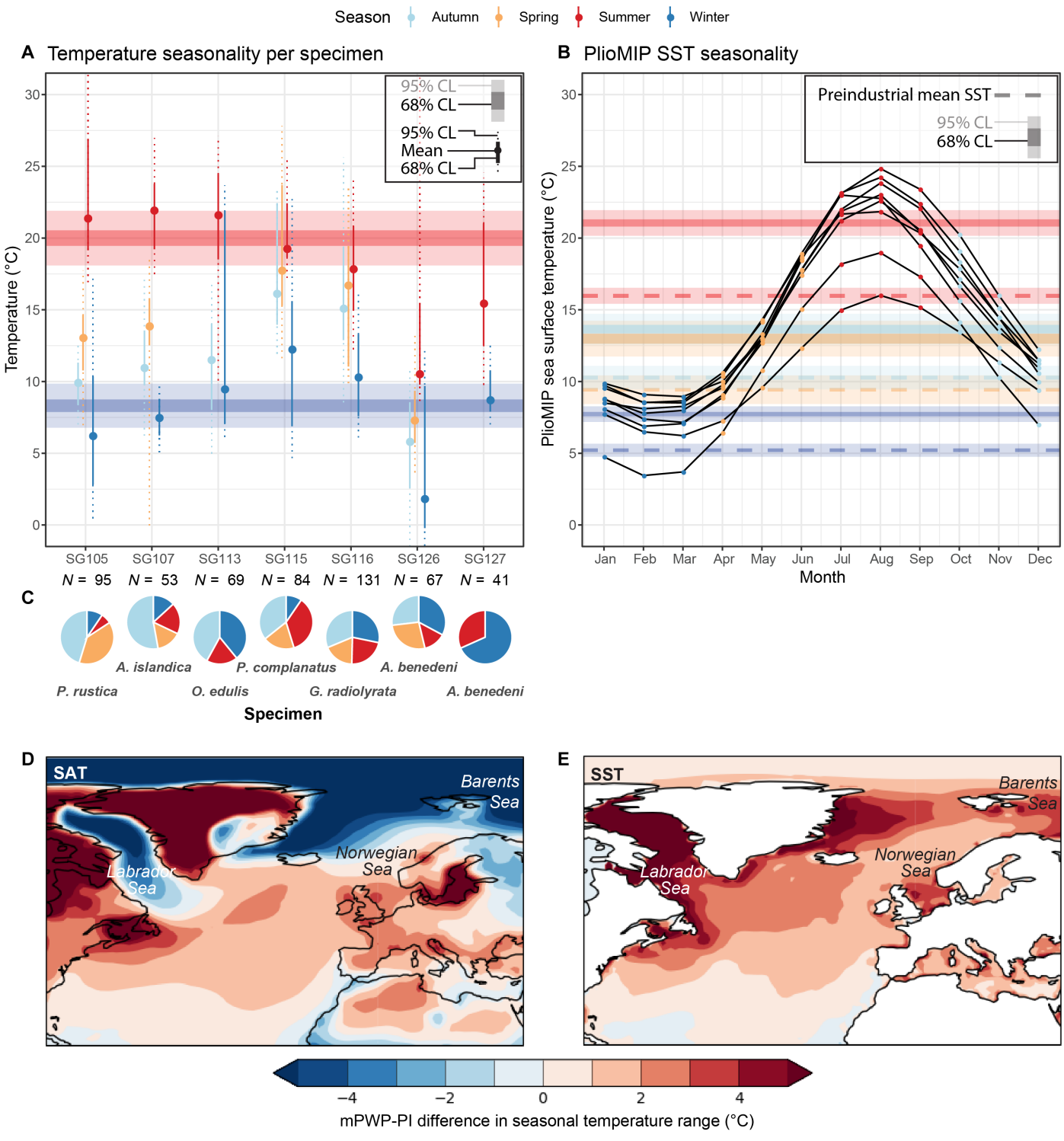

Fig. 2. Data-model comparison. (**A**) Weighted mean seasonal temperatures per specimen (filled circles with solid and vertical dotted lines indicating 68 and 95% confidence intervals, respectively) and summer and winter temperatures based on the complete dataset (horizontal shaded bars in red and blue, respectively) with propagated uncertainties [68 and 95% confidence level (CL); see Materials and Methods]. Horizontal dashed lines in the same colors indicate mean preindustrial SNS SST. (**B**) Local monthly SST outcomes of individual PlioMIP2 models with winter (January to March; blue) and summer (July to September; red) temperature estimates (horizontal shaded bars showing 68 and 95% CL). Dashed lines in the same colors indicate mean SST outcomes [with uncertainty; 95% CL (*9*)] from preindustrial control simulations using the same models. (**C**) Clumped isotope sample sizes and seasonal representation of samples per specimen. (**D** and **E**) Spatial variability in the difference in seasonal contrast (July to January) in SAT(D) and SST (E), respectively, between PlioMIP2 multi-model mean mPWP runs and PlioMIP2 preindustrial (PI) control runs of the same models.

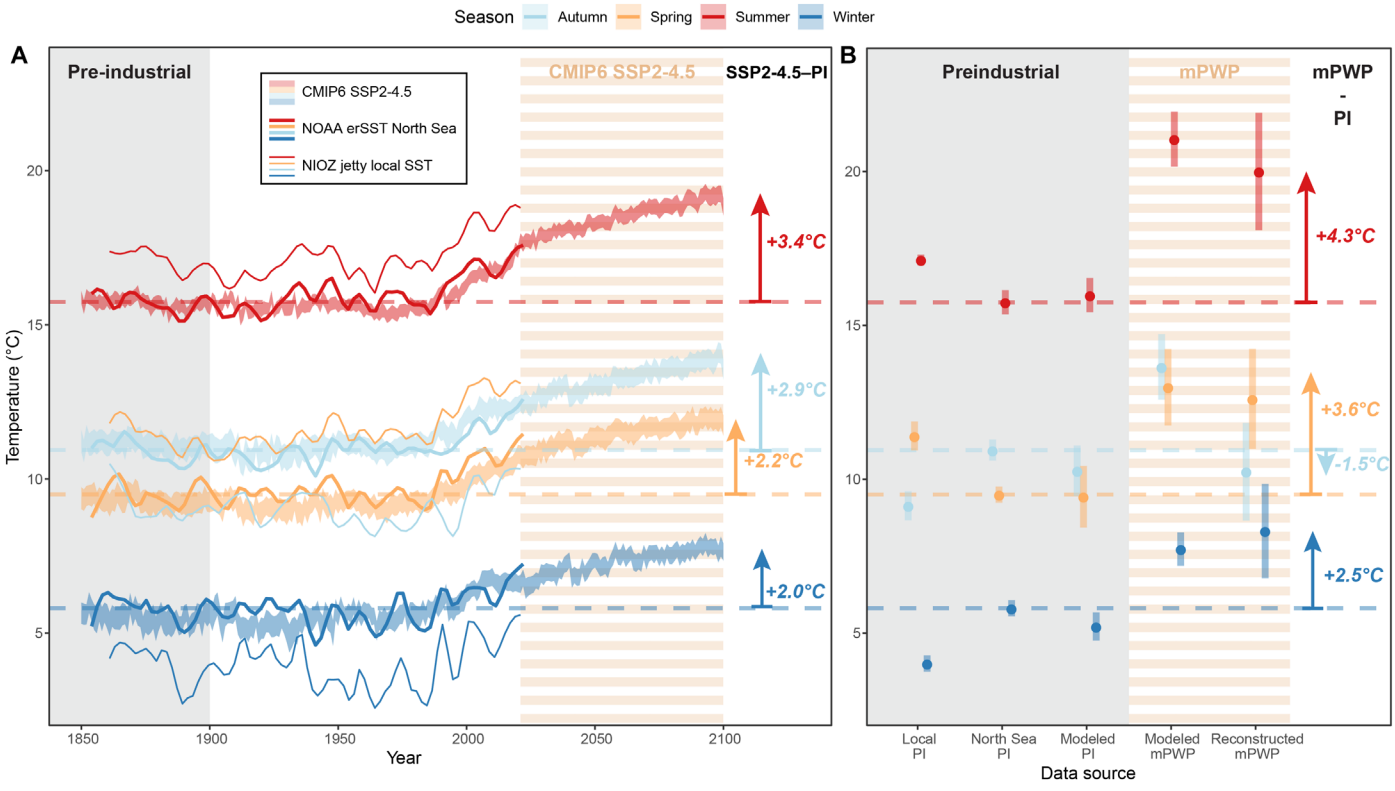

Fig. 3. Pliocene reconstructions inform future climate projections. (**A**) Seasonal local (NIOZ jetty, Texel, The Netherlands) SST measurements (thin solid lines; LOESS-smoothed with span of 10% of the record), National Oceanic and Atmospheric Administration Extended Reconstructed SST v5 (NOAA ERSSTv5) averages for the SNS (thick solid lines; LOESS-smoothed with span of 10% of the record), and CMIP6 SSP2-4.5 scenario transient SNS SST simulations (shaded area) between 1850 and 2100. Arrows and figures on the right indicate temperature differences between CMIP6 SSP2-4.5 projections for 2100 CE and preindustrial SNS SSTs (dashed lines). (**B**) Preindustrial (before 1900 CE) seasonal SST averages based on historical SST records [NOAA ERSSTv5 (*41*) SNS averages and NIOZ jetty local record (*42*)] and PlioMIP2 preindustrial model outcomes are compared with mPWP seasonality based on PlioMIP2 mPWP model simulations and mollusk-based reconstructions. Arrows and figures on the right indicate seasonal temperature differences between mollusk-based mPWP temperature reconstructions and preindustrial SNS SST (dashed lines). The gray background color indicates the preindustrial reference period (1850 to 1900 CE), while horizontal orange and white banding indicates the CMPI6 SSP2-4.5 model projections and mPWP model outcomes and reconstructions.

projections of European climate for the year 2100. This approach offers a detailed glimpse of the potential future climate in Europe under a moderate emission scenario.

RESULTS

Data-model agreement on enhanced summer warming in the North Sea

Aggregated results from all bivalve specimens give weighted winter (8.3° ± 1.5°C), spring (12.6° ± 1.6°C), summer (20.0° ± 1.9°C), and autumn (10.2° ± 1.6°C) SST averages during the mPWP in the SNS (Fig. 2A). The reconstructed winter and summer temperatures agree with winter (January to March; 7.7° ± 0.5°C) and summer (July to September; 21.1° ± 0.9°C) temperatures in the SNS from aggregated PlioMIP2 model results (Fig. 2B). Both reconstructed and modeled winter and summer temperatures are significantly higher than winter (5.2° ± 0.9°C) and summer (16.0° ± 0.6°C) temperatures in preindustrial (280 ppmV CO_2) PlioMIP2 control runs and instrumental records (Fig. 2, A and B). Our reconstructions yield 2.5° ± 1.5°C warmer winters and 4.3° ± 1.9°C warmer summers during the mPWP compared to mean winter (5.8° ± 0.3°C) and summer (15.7° ± 0.4°C) temperatures in the SNS over the period 1854 to 1900 CE [Fig. 3A; based on National Oceanic and Atmospheric Administration Extended Reconstructed SST v5 (NOAA ERSSTv5) (*41*)].

Locally elevated spring temperatures

Intriguingly, mollusk-based reconstructions yield significantly higher spring (April to June; 12.6° ± 1.6°C) than autumn (October to December; 10.2° ± 1.6°C) temperatures during the mPWP. This contrasts with regional SNS SST averages from both preindustrial (spring: 9.4° ± 1.0°C; autumn: 10.3° ± 0.8°C) and mPWP (spring: 13.0° ± 1.2°C; autumn: 13.6° ± 1.1°C) PlioMIP2 model runs as well as ERSST SNS SST averages (spring: 9.5° ± 0.3°C; autumn: 10.9° ± 0.3°C), which consistently yield higher temperatures in autumn compared to spring. Contrarily, local preindustrial instrumental SST time series from the Netherlands Institute for Sea Research (NIOZ) monitoring station on the SNS coast [island of Texel, northwestern Netherlands (*42*); see Fig. 1, A and B; Supplementary Methods] do exhibit significantly elevated spring (11.4° ± 0.5°C) compared to autumn (9.1° ± 0.5°C) temperatures. Shallow coastal waters, such as the tidal flats of the Wadden Sea close to the NIOZ monitoring station, are highly responsive to air temperature, which leads to elevated SSTs in the spring season, while

more offshore areas of the North Sea have higher thermal inertia, explaining elevated autumn temperatures (*42*). The elevated spring and reduced autumn SST reconstructions thus highlight that the mollusk shells record detailed seasonal SST variability in the coastal SNS during the mPWP.

Interspecimen variability

Reconstructed seasonal temperatures vary between fossil shell specimens, with some specimens recording warmer temperatures (e.g., *Pecten complanatus*; SG115; winter: 12.3° ± 4.4°C; summer: 19.3° ± 1.8°C) and others cooler temperatures (e.g., *Angulus benedeni benedeni*; SG126 and SG127; winter: 1.9° ± 4.9°C; summer: 15.5° ± 4.3°C; Fig. 2A). These interspecimen differences probably occur due to the occurrence of growth halts and variations in growth rates between seasons (Fig. 2C) and between consecutive growth years (see figs. S13 to S26), which dampen seasonality due to the averaging of samples around the seasonal extreme. In addition, variability between specimens may arise from differences in the seasonal temperature range within their age range (2.7 to 3.3 Ma; see Fig. 1C). The latter may explain the relatively warm spring temperatures recorded by specimens SG115 and SG116 from the *Cultellus* level and comparatively cooler temperatures recorded by SG126 and SG127 from the *benedeni* level at the top of the Oorderen Member (see table S1). Our weighted averages of summer and winter temperatures (Fig. 2A) ensure that this interspecimen variability does not bias the reconstructions.

PlioMIP2 models reproduce SST seasonality in the modern North Sea

Transient simulations of SNS SST seasonality from before the Industrial Revolution (1850 CE) to present day (2023 CE) by the CMIP6 model ensemble (*6*) mimic historical SST records from the region (Fig. 3A) (*41*). Seasonal SNS SST simulations by the PlioMIP2 model ensemble under preindustrial radiative forcing (*9*) (winter: 5.2° ± 0.5°C; summer: 16.0° ± 0.6°C) closely resemble preindustrial (1850 to 1900 CE) CMIP6 seasonal SNS SST simulations (winter: 5.5° ± 0.3°C; summer: 15.7° ± 0.7°C) and historical winter (5.8° ± 0.3°C) and summer SNS SST (15.7° ± 0.4°C) records (Fig. 3B) (*41*). Local SST records from the NIOZ monitoring station in Texel (*42*) reveal slightly higher seasonal SST ranges (winter: 4.0° ± 0.3°C; summer: 17.1° ± 0.2°C; Fig. 3B), which are well explained by their coastal location (see above). This agreement shows that PlioMIP2 models successfully reproduce summer and winter SSTs in the SNS.

The mid- to high-latitude seasonal temperature response to mPWP-like warming

Maps of PlioMIP2 seasonal SST outcomes show that the enhanced seasonal contrast observed in our reconstructions is present throughout the mid-latitudes to high latitudes in the North Atlantic (Fig. 2E). Enhanced SST seasonality is more pronounced in areas that are characterized by high seasonal contrast in surface air temperature (SAT) and cold winters (e.g., Labrador Sea and Barents Sea) than in regions with milder winters (e.g., Norwegian Sea). Contrarily, SAT only shows enhanced seasonal contrast in the mid-latitudes under mPWP conditions (Fig. 2D). Areas with the strongest enhanced seasonal SST contrast (e.g., Labrador Sea and Barents Sea; Fig. 2E) show a reduced seasonal SAT contrast under mPWP conditions compared to the preindustrial control runs (Fig. 2D). PlioMIP2 model simulations of sea ice extent (fig. S33) show that these regions where the SST and SAT seasonality respond differently to mPWP-scale warming are characterized by winter sea ice cover in preindustrial runs. They lose much of their winter sea ice under mPWP conditions; a 53% decrease in mean annual sea ice extent during the mPWP compared to preindustrial climate is simulated in PlioMIP2 models (*43*). Contrarily, areas with enhanced summer warming in both SST and SAT are sea ice–free year round in both mPWP and preindustrial model runs. SAT seasonality over land (both in North America and Europe; Fig. 2D) is enhanced at both mid-latitudes and high latitudes, following the SST pattern. PlioMIP2 model outcomes show that summer cloud cover is severely reduced in the mid-latitudes of the North Atlantic, where both SST and SAT seasonality is enhanced (figs. S34 and S35).

DISCUSSION

Recent terrestrial mPWP data-model comparisons highlight that PlioMIP2 models cannot reproduce the full extent of the mPWP warming that data suggest (*2*, *21*, *44*). Likewise, in both the pelagic and terrestrial realm, reconstruction of the full seasonal cycle is challenging due to proxy limitations (*2*, *21*). Detailed temperature monitoring studies show that shallow marine temperatures are strongly linked to air temperatures and local weather systems (*45*). Together with the enhanced occurrence of summer stratification in warmer climates (*24*, *46*, *47*), a change in atmospheric circulation patterns may drive the summer increase in SST during the mPWP and in the future observed in data and models (Figs. 2 and 3). The seasonal cycle is much more pronounced in the terrestrial realm, which could explain part of the large seasonal data-model mismatch at terrestrial Northern Hemisphere high latitudes (*21*).

PlioMIP2 models closely agree with mollusk-based reconstructions of SNS summer and winter SST during the mPWP (Figs. 2 and 3B). The summer warming observed in SST data and model outcomes is also reflected in PlioMIP2 SAT seasonality in the SNS region (Fig. 2D and fig. S37). This highlights that PlioMIP2 models can reconstruct seasonal SST variability in the North Atlantic despite the difficulties with terrestrial data-model comparisons (*21*). However, large intermodel variability in regions with poor data-model agreement suggests that structural model uncertainties also contribute to the mismatch (*21*).

The agreement between PlioMIP2 preindustrial control simulations and present-day climate (represented in CMIP6 models and instrumental records; Fig. 3) (*1*, *9*, *48*) lends confidence to the application of mPWP reconstructions and model simulations to better understand the seasonal impact of moderate global warming on future European climate. The seasonal-scale data-model agreement in the SNS, situated between the pelagic and terrestrial realms, for both present-day and mPWP climate, sheds light on the seasonal response to warmer climate in the mid-latitudes: The unique potential of marine mollusks to record seasonal-scale SST variability in coastal regions (*28*, *49*) in combination with the strong relationship between mid-latitude coastal SST and SAT (*45*, *50*) (see Fig. 2D and figs. S28 and S32) highlights the key role of seasonally resolved shallow marine climate archives for better understanding past and future climates.

Our mollusk-based data and PlioMIP2 model estimates of mPWP SST seasonality resemble projections of future (2081 to 2100 CE) SNS winter (7.7° ± 0.3°C) and summer SST (19.1° ± 0.5°C; Fig. 3A) by transient CMIP6 model simulations of the "middle-of-the-road" SSP2-4.5 scenario (Fig. 3) (*48*). Note that these are two different climate scenarios: CMIP6 represents a transient climate disturbance, while the mPWP simulations and reconstructions sample an

equilibrated climate under long-term atmospheric CO_2 forcing of 400 ppmV (*9*). The difference is evident from atmospheric PCO_2 (partial pressure of CO_2) projections of ~600 ppmV in 2100 CE and ~580 ppmV in the long term (2500 CE) under SSP2-4.5, which notably exceed the mPWP estimate of ~400 ppmV (*3*, *5*). Notwithstanding this difference, the results of our data-model comparison and the similarity of the SSP2-4.5 scenario to the current global emission trajectory (*4*) show that the mPWP presents valuable lessons for climate in Europe by the end of this century and models are able to project seasonal climate in this region in a warmer world.

The spatial variability in seasonal response to mPWP warming of SST and SAT reveals a clear signature of sea ice extent: SST and SAT respond in opposite directions to mPWP warming in the higher-latitude areas that lose winter sea ice cover under mPWP conditions (Fig. 2, D and E; e.g., Labrador Sea and Barents Sea; fig. S33). The loss of winter sea ice in an mPWP-like climate scenario facilitates heat transfer from the upper ocean to the lower atmosphere in winter, cooling the upper ocean in winter (enhancing SST seasonality) and warming the lower atmosphere [reducing SAT seasonality; as demonstrated in (*43*)]. This effect explains why higher latitudes are more affected by the sea ice–albedo feedback, which changes due to a reduction in sea ice extent under mPWP-like conditions (*51*, *52*) and in future climate scenarios (*53*). In these regions, Arctic amplification is expected to cause winter SAT to warm faster than other regions (*10*, *54*), while SST actually shows a summer warming effect in both the high latitudes and mid-latitudes.

This hypothesis is supported by climate models showing that Arctic amplification reduces the latitudinal SAT gradient in warmer climates (*10*). This mechanism has been demonstrated to weaken the mid-latitude atmospheric summer circulation in the present-day climate, causing a weakening of storm tracks, with lower cyclone activity over Europe, more persistent weather conditions, and a reduction in summer cloud cover (*11*). This reduction in cloud cover over temperate latitudes of the North Atlantic is also simulated in PlioMIP2 model outcomes (fig. S35) (*13*), thus suggesting that a similar mechanism causes the seasonal temperature structure in the mPWP. Recent observations from various parts of the North Atlantic region suggest that circulation changes are already enhancing summer warming and prolonging heat waves through low cyclone activity, low cloud cover, and more persistent weather conditions (*12*, *55*, *56*). In the winter months, zonal (westerly) wind increases, enhancing cloud cover and precipitation and suppressing winter warming (*13*). Together, these changes in the atmospheric circulation regime result in an increase in extreme weather conditions in Europe in both seasons, with more severe precipitation events in winter and more prolonged droughts in summer (*13*).

Our data-model analysis reveals that an mPWP-scale SST increase in the SNS region causes more pronounced warming in summer (reconstructions: +4.3° ± 1.9°C; PlioMIP2 models: +5.1° ± 0.9°C) than in winter (reconstructions: +2.5° ± 1.5°C; PlioMIP2 models: +2.5° ± 0.5°C; Fig. 3B). Historical climate data (Fig. 3A) and recent climate attribution studies (*57*–*59*) reveal that this trend is already underway in Europe (*60*). Therefore, reconstructions and model simulations of mPWP seasonality reveal the impact of our current climate trajectory: Because of the hypothesized mid-latitude circulation changes, global warming is likely to regionally shift the distribution of extreme weather events on top of the overall increase in frequency and severity of these events due to the thermodynamic effect of greenhouse warming (*14*). The seasonally asymmetric change in mid-latitude zonal circulation, even under a relatively mild mPWP-like warming scenario, renders Europe particularly vulnerable to prolonged heat and drought in summer and intense precipitation events in winter (*13*). Enhanced summer warming in coastal regions poses a serious risk for shallow marine communities since it leads to more frequent and extreme weather events, such as marine heat waves (*29*, *30*, *57*, *59*, *61*). These marine heat waves (*62*) have recently caused mass mortality events (*63*), mass coral bleaching (*64*), and toxic algal blooms (*65*), severely affecting marine biodiversity. They are among the major reasons for concern related to anthropogenic climate change (*66*). Considering the high societal and ecological importance of mid-latitude coastal regions, local data-model comparison studies of short-term variability during past climates relevant for future warming scenarios play a fundamental role in honing the model projections that inform climate adaptation strategies.

MATERIALS AND METHODS

Specimen collection

Seven fossil mollusk specimens were collected by one of the authors (S.G.) for analysis from temporary exposures of the Oorderen Member of the Lillo Formation in the Antwerp area (Belgium; see Fig. 1). These were specimens of *A. benedeni benedeni* (specimen ID: SG126 and SG127) from Deurganckdoksluis (51°16′49″N, 4°14′56″E; collected in 2013), *P. complanatus* (SG115) and *Glycymeris radiolyrata* (SG116) from Deurganckdok (51°17′24″N, 4°15′37″E; collected on 2 February 2001), and *Pygocardia rustica* (SG105), *Ostrea edulis* (SG113), and *Arctica islandica* (SG107) from Verrebroekdok (51°16′16″N, 4°12′53″E; collected in 1999–2000). At these localities, the Oorderen Member, from bottom to top, is divided into basal shell bed, *Atrina* level, *Cultellus* level (SG115 and SG116), and *benedeni* level (SG126 and SG127) (*37*). Specimens SG105, SG113, and SG107 were collected ex situ within the Oorderen Member. The estimated age range for the Oorderen Member is 2.72 to 3.3 Ma (see Fig. 1) (*35*, *67*).

Paleoenvironmental context

Field observations and a detailed assessment of the composition of the invertebrate fauna reveal that the fossil-bearing sediments of the Oorderen Member were deposited between 30 and 50 m water depth during warm, highstand intervals (*35*, *36*). Previous studies have argued that the SNS undergoes summer stratification during the mPWP, which would cause molluscan shell reconstructions to underestimate summer temperatures (*24*, *47*). However, the lack of dysoxic faunas in the Oorderen Member suggests the absence of persistent stratification (*35*). Furthermore, the presence of sedimentary structures indicative of tidal currents and strong vertical mixing during deposition of the Oorderen Member argues against a large surface to seafloor temperature gradient (*39*). Therefore, it is likely that the mollusks recorded temperatures close to the SSTs year round. This assessment is supported by the evidence of warm spring and cool autumn temperatures, suggesting a direct response of the water temperature experienced by the mollusks to the seasonal cycle in SATs (see Results; Fig. 3). However, we cannot fully exclude that spatially and temporally restricted temperature stratification did occur during the lifetime of the studied specimens (*24*, *47*). Note that, even if summer stratification occurred, the summer temperatures recorded by the mollusks would underestimate the true mPWP summer SST and the occurrence of enhanced summer warming during the mPWP would still be supported by the data.

Specimen preparation

Shells were partially embedded in epoxy resin before polished thick sections were prepared to expose a cross section through the axis of maximum shell growth [following (*68*); see fig. S3]. Preservation of the original shell calcite and aragonite was verified using a combination of scanning electron microscopy (SEM), cathodoluminescence microscopy, electron backscatter diffraction microscopy (EBSD), micro–x-ray fluorescence (μXRF), and x-ray diffraction [XRD; see (*67*) and figs. S4 to S12]. Only shells with excellent preservation as demonstrated by these methods were considered for clumped isotope analysis.

Geochemical analysis

Carbonate was sampled along transects in the direction of growth in transects on cross sections through the outer shell layers of all shells except *P. complanatus* (SG115) and *A. benedeni benedeni* (SG126 and SG127), whose thin outer shell layers necessitated sampling on the outside of the shell. A combination of handheld drilling (outside) and micromilling (in transects) was used to sample along narrow growth increments to minimize time averaging (Supplementary Materials). The number of replicates per specimen ranges from 61 to 157 (Fig. 2): SG105, $n = 98$; SG107, $n = 63$; SG113, $n = 90$; SG115, $n = 100$; SG116, $n = 157$; SG126, $n = 79$; SG127, $n = 61$. Some samples were replicated more than once, causing multiple replicates to originate from the same location in the shell, and some of these replicate measurements were discarded as outliers during data processing (see below). Measurements from *A. benedeni benedeni* (SG126 and SG127) include data from (*67*) as well as additional analyses on the same specimens carried out for this study. Small (70 to 160 μg) aliquots of each sample were digested in phosphoric acid for 600 s at 70°C in a Kiel IV carbonate preparation device, after which the resultant CO_2 gas was purified using two cold fingers and a Porapak trap (*69*) before the clumped isotope composition (Δ_{47}) was analyzed using two Thermo MAT253 mass spectrometers. A long-integration dual-inlet (LIDI) workflow (*69*, *70*) was used for all except 53 aliquots from *P. rustica* (SG105); the latter aliquots were measured using sample-standard measurement cycles ["click-clack" mode; e.g., (*71*)]. Clumped isotopic ratios were corrected for intensity-based Δ_{47} offsets based on intensity-matched ETH-3 standards (see section S3.1) before being standardized using the ETH standards (*72*), which were run in approximately 1:1 ratio with the samples (*73*) and corrected for ^{17}O concentration following (*74*). Long-term analytical precision was monitored using IAEA-C2 and Merck reference materials (typical standard deviation of 0.04‰; see table S2) after outlier removal based on metadata on instrument performance (see criteria in section S3.2).

Seasonality reconstructions

For each mollusk specimen, samples were internally dated relative to the seasonal cycle using ShellChron (*75*), after which measurements within a specimen were grouped in four 3-monthly bins ("seasons"). Summer was defined as the consecutive 3-month period with the lowest mean Δ_{47} value, calculated separately for each specimen (see section S3.2 and figs. S20 to S32). The fact that these 3-monthly bins do not always line up with the minima and maxima in the stable oxygen isotope profiles through the shells shows that the common assumption that these extreme stable oxygen isotope values represent summer and winter seasons does not always hold true [see (*76*)]. Mean seasonal Δ_{47} values were obtained through weighted averages of seasonal means and uncertainties considering uncertainty within and variability between specimens. Seasonal temperatures during the mPWP were reconstructed from Δ_{47} for each seasonal group using the clumped isotope calibration by (*77*), propagating uncertainty on Δ_{47} values following the procedure described in the supplement of (*78*).

Climate model output

Seasonal SST from the SNS was extracted from the corresponding local ocean grid cells (51°N to 55°N, 2°E to 4°E) in the PlioMIP2 model ensemble (see Fig. 2). SNS SST records were obtained from the same area within the ERSSTv5 product (*41*) and supplemented with local SST observations from the NIOZ monitoring station (*42*). Future projections matching the SSP2-4.5 scenario (*48*) were produced for CMIP6, and the regional SST outcomes were exported from the Intergovernmental Panel on Climate Change (IPCC) WG1 Interactive Atlas (*79*). Seasons were defined as weighted means of the 3 months containing the largest number of days in the season according to the astronomical definition: winter: January to March; spring: April to June; summer: July to September; autumn: October to December. Data processing was carried out using the open-source computational software R (*80*), and scripts are provided in (*81*).

Supplementary Materials

This PDF file includes:

Supplementary Text
Figs. S1 to S46
Tables S1 to S5
References

REFERENCES AND NOTES

1. A. M. Haywood, H. J. Dowsett, A. M. Dolan, Integrating geological archives and climate models for the mid-Pliocene warm period. *Nat. Commun.* **7**, 10646 (2016).
2. H. J. Dowsett, K. M. Foley, D. K. Stoll, M. A. Chandler, L. E. Sohl, M. Bentsen, B. L. Otto-Bliesner, F. J. Bragg, W.-L. Chan, C. Contoux, A. M. Dolan, A. M. Haywood, J. A. Jonas, A. Jost, Y. Kamae, G. Lohmann, D. J. Lunt, K. H. Nisancioglu, A. Abe-Ouchi, G. Ramstein, C. R. Riesselman, M. M. Robinson, N. A. Rosenbloom, U. Salzmann, C. Stepanek, S. L. Strother, H. Ueda, Q. Yan, Z. Zhang, Sea surface temperature of the mid-Piacenzian ocean: A data-model comparison. *Sci. Rep.* **3**, 2013 (2013).
3. E. de la Vega, T. B. Chalk, P. A. Wilson, R. P. Bysani, G. L. Foster, Atmospheric CO2 during the Mid-Piacenzian Warm Period and the M2 glaciation. *Sci. Rep.* **10**, 1–8 (2020).
4. IPCC, *Climate Change 2021: The Physical Science Basis. Contribution of Working Group I to the Sixth Assessment Report of the Intergovernmental Panel on Climate Change* (Cambridge Univ. Press, 2021).
5. M. Meinshausen, Z. R. J. Nicholls, J. Lewis, M. J. Gidden, E. Vogel, M. Freund, U. Beyerle, C. Gessner, A. Nauels, N. Bauer, J. G. Canadell, J. S. Daniel, A. John, P. B. Krummel, G. Luderer, N. Meinshausen, S. A. Montzka, P. J. Rayner, S. Reimann, S. J. Smith, M. van den Berg, G. J. M. Velders, M. K. Vollmer, R. H. J. Wang, The shared socio-economic pathway (SSP) greenhouse gas concentrations and their extensions to 2500. *Geosci. Model Dev.* **13**, 3571–3605 (2020).
6. Y. Liang, N. P. Gillett, A. H. Monahan, Climate model projections of 21st century global warming constrained using the observed warming trend. *Geophys. Res. Lett.* **47**, e2019GL086757 (2020).
7. K. D. Burke, J. W. Williams, M. A. Chandler, A. M. Haywood, D. J. Lunt, B. L. Otto-Bliesner, Pliocene and Eocene provide best analogs for near-future climates. *Proc. Natl. Acad. Sci. U.S.A.* **115**, 13288–13293 (2018).
8. Climate Action Tracker, 2100 Warming Projections: Emissions and expected warming based on pledges and current policies, 2022; https://climateactiontracker.org/global/temperatures/.
9. A. M. Haywood, J. C. Tindall, H. J. Dowsett, A. M. Dolan, K. M. Foley, S. J. Hunter, D. J. Hill, W.-L. Chan, A. Abe-Ouchi, C. Stepanek, G. Lohmann, D. Chandan, W. R. Peltier, N. Tan, C. Contoux, G. Ramstein, X. Li, Z. Zhang, C. Guo, K. H. Nisancioglu, Q. Zhang, Q. Li, Y. Kamae, M. A. Chandler, L. E. Sohl, B. L. Otto-Bliesner, R. Feng, E. C. Brady, A. S. Von der Heydt, M. L. J. Baatsen, D. J. Lunt, The Pliocene Model Intercomparison Project Phase 2: Large-scale climate features and climate sensitivity. *Clim. Past* **16**, 2095–2123 (2020).

10. J. Cohen, J. A. Screen, J. C. Furtado, M. Barlow, D. Whittleston, D. Coumou, J. Francis, K. Dethloff, D. Entekhabi, J. Overland, J. Jones, Recent Arctic amplification and extreme mid-latitude weather. *Nat. Geosci.* **7**, 627–637 (2014).
11. D. Coumou, J. Lehmann, J. Beckmann, The weakening summer circulation in the Northern Hemisphere mid-latitudes. *Science* **348**, 324–327 (2015).
12. S. Hofer, A. J. Tedstone, X. Fettweis, J. L. Bamber, Decreasing cloud cover drives the recent mass loss on the Greenland Ice Sheet. *Sci. Adv.* **3**, e1700584 (2017).
13. E. Rousi, F. Selten, S. Rahmstorf, D. Coumou, Changes in North Atlantic atmospheric circulation in a warmer climate favor winter flooding and summer drought over Europe. *J. Clim.* **34**, 2277–2295 (2021).
14. D. Coumou, G. Di Capua, S. Vavrus, L. Wang, S. Wang, The influence of Arctic amplification on mid-latitude summer circulation. *Nat. Commun.* **9**, 2959 (2018).
15. H. J. Dowsett, A. M. Haywood, P. J. Valdes, M. M. Robinson, D. J. Lunt, D. J. Hill, D. K. Stoll, K. M. Foley, Sea surface temperatures of the mid-Piacenzian Warm Period: A comparison of PRISM3 and HadCM3. *Palaeogeogr. Palaeoclimatol. Palaeoecol.* **309**, 83–91 (2011).
16. T. D. Herbert, L. C. Peterson, K. T. Lawrence, Z. Liu, Tropical ocean temperatures over the past 3.5 million years. *Science* **328**, 1530–1534 (2010).
17. K. T. Lawrence, S. Sosdian, H. E. White, Y. Rosenthal, North Atlantic climate evolution through the Plio-Pleistocene climate transitions. *Earth Planet. Sci. Lett.* **300**, 329–342 (2010).
18. J. C. Wit, G.-J. Reichart, S. J. A. Jung, D. Kroon, Approaches to unravel seasonality in sea surface temperatures using paired single-specimen foraminiferal δ18O and Mg/Ca analyses. *Paleoceanography* **25**, PA4220 (2010).
19. G. Jia, X. Wang, W. Guo, L. Dong, Seasonal distribution of archaeal lipids in surface water and its constraint on their sources and the TEX86 temperature proxy in sediments of the South China Sea. *J. Geophys. Res. Biogeo.* **122**, 592–606 (2017).
20. M. H. Conte, M.-A. Sicre, C. Rühlemann, J. C. Weber, S. Schulte, D. Schulz-Bull, T. Blanz, Global temperature calibration of the alkenone unsaturation index (UK′37) in surface waters and comparison with surface sediments. *Geochem. Geophys. Geosyst.* **7**, Q02005 (2006).
21. J. C. Tindall, A. M. Haywood, U. Salzmann, A. M. Dolan, T. Fletcher, The warm winter paradox in the Pliocene northern high latitudes. *Clim. Past* **18**, 1385–1405 (2022).
22. D. K. Moss, L. C. Ivany, D. S. Jones, Fossil bivalves and the sclerochronological reawakening. *Paleobiology* **47**, 551–573 (2021).
23. B. R. Schöne, J. Fiebig, Seasonality in the North Sea during the Allerød and Late Medieval Climate Optimum using bivalve sclerochronology. *Int. J. Earth Sci.* **98**, 83–98 (2009).
24. A. L. A. Johnson, A. M. Valentine, B. R. Schöne, M. J. Leng, S. Goolaerts, Sclerochronological evidence of pronounced seasonality from the late Pliocene of the southern North Sea basin and its implications. *Clim. Past* **18**, 1203–1229 (2022).
25. D. J. Reynolds, J. D. Scourse, P. R. Halloran, A. J. Nederbragt, A. D. Wanamaker, P. G. Butler, C. A. Richardson, J. Heinemeier, J. Eirikkson, K. L. Knudsen, Annually resolved North Atlantic marine climate over the last millennium. *Nat. Commun.* **7**, 13502 (2016).
26. D. Bajnai, J. Fiebig, A. Tomašových, S. Milner Garcia, C. Rollion-Bard, J. Raddatz, N. Löffler, C. Primo-Ramos, U. Brand, Assessing kinetic fractionation in brachiopod calcite using clumped isotopes. *Sci. Rep.* **8**, 1–12 (2018).
27. N. J. de Winter, J. Vellekoop, R. Vorsselmans, A. Golreihan, J. Soete, S. V. Petersen, K. W. Meyer, S. Casadio, R. P. Speijer, P. Claeys, An assessment of latest Cretaceous *Pycnodonte vesicularis* (Lamarck, 1806) shells as records for palaeoseasonality: A multi-proxy investigation. *Clim. Past* **14**, 725–749 (2018).
28. L. C. Ivany, Reconstructing paleoseasonality from accretionary skeletal carbonates—Challenges and opportunities. *Paleontol. Soc. Papers* **18**, 133–166 (2012).
29. D. A. Smale, T. Wernberg, E. C. J. Oliver, M. Thomsen, B. P. Harvey, S. C. Straub, M. T. Burrows, L. V. Alexander, J. A. Benthuysen, M. G. Donat, M. Feng, A. J. Hobday, N. J. Holbrook, S. E. Perkins-Kirkpatrick, H. A. Scannell, A. Sen Gupta, B. L. Payne, P. J. Moore, Marine heatwaves threaten global biodiversity and the provision of ecosystem services. *Nat. Clim. Change* **9**, 306–312 (2019).
30. J. Garrabou, D. Gómez-Gras, A. Medrano, C. Cerrano, M. Ponti, R. Schlegel, N. Bensoussan, E. Turicchia, M. Sini, V. Gerovasileiou, N. Teixido, A. Mirasole, L. Tamburello, E. Cebrian, G. Rilov, J.-B. Ledoux, J. B. Souissi, F. Khamassi, R. Ghanem, M. Benabdi, S. Grimes, O. Ocaña, H. Bazairi, B. Hereu, C. Linares, D. K. Kersting, G. la Rovira, J. Ortega, D. Casals, M. Pagès-Escolà, N. Margarit, P. Capdevila, J. Verdura, A. Ramos, A. Izquierdo, C. Barbera, E. Rubio-Portillo, I. Anton, P. López-Sendino, D. Díaz, M. Vázquez-Luis, C. Duarte, N. Marbà, E. Aspillaga, F. Espinosa, D. Grech, I. Guala, E. Azzurro, S. Farina, M. Cristina Gambi, G. Chimienti, M. Montefalcone, A. Azzola, T. P. Mantas, S. Fraschetti, G. Ceccherelli, S. Kipson, T. Bakran-Petricioli, D. Petricioli, C. Jimenez, S. Katsanevakis, I. T. Kizilkaya, Z. Kizilkaya, S. Sartoretto, R. Elodie, S. Ruitton, S. Comeau, J.-P. Gattuso, J.-G. Harmelin, Marine heatwaves drive recurrent mass mortalities in the Mediterranean Sea. *Glob. Change Biol.* **28**, 5708–5725 (2022).
31. S. Manes, M. J. Costello, H. Beckett, A. Debnath, E. Devenish-Nelson, K.-A. Grey, R. Jenkins, T. M. Khan, W. Kiessling, C. Krause, S. S. Maharaj, G. F. Midgley, J. Price, G. Talukdar, M. M. Vale, Endemism increases species' climate change risk in areas of global biodiversity importance. *Biol. Conserv.* **257**, 109070 (2021).
32. A. Toimil, I. J. Losada, R. J. Nicholls, R. A. Dalrymple, M. J. F. Stive, Addressing the challenges of climate change risks and adaptation in coastal areas: A review. *Coas. Eng.* **156**, 103611 (2020).
33. D. Huyghe, M. Daëron, M. de Rafelis, D. Blamart, M. Sébilo, Y.-M. Paulet, F. Lartaud, Clumped isotopes in modern marine bivalves. *Geochim. Cosmochim. Acta* **316**, 41–58 (2022).
34. N. J. de Winter, R. Witbaard, I. J. Kocken, I. A. Müller, J. Guo, B. Goudsmit, M. Ziegler, Temperature dependence of clumped isotopes (Δ47) in aragonite. *Geophys. Res. Lett.* **49**, e2022GL099479 (2022).
35. F. P. Wesselingh, F. S. Busschers, S. Goolaerts, Observations on the Pliocene sediments exposed at Antwerp International Airport (northern Belgium) constrain the stratigraphic position of the Broechem fauna. *Geol. Belgica* **23**, 315–321 (2020).
36. R. Marquet, Ecology and evolution of Pliocene bivalves from the Antwerp Basin. *Bull. Inst. R. Sci. Nat. Belg. Sci. Terre* **74**, 205–212 (2004).
37. N. Vandenberghe, S. Louwye, An introduction to the Neogene stratigraphy of northern Belgium: Present status. *Geol. Belgica* **23**, 97–112 (2020).
38. M. Quante, F. Colijn, *North Sea Region Climate Change Assessment* (Springer Nature, 2016).
39. J. Deckers, S. Louwye, S. Goolaerts, The internal division of the Pliocene Lillo Formation: Correlation between Cone Penetration Tests and lithostratigraphic type sections. *Geol. Belgica* **23**, 333–343 (2020).
40. A. M. Haywood, H. J. Dowsett, A. M. Dolan, D. Rowley, A. Abe-Ouchi, B. Otto-Bliesner, M. A. Chandler, S. J. Hunter, D. J. Lunt, M. Pound, U. Salzmann, The Pliocene Model Intercomparison Project (PlioMIP) Phase 2: Scientific objectives and experimental design. *Clim. Past* **12**, 663–675 (2016).
41. B. Huang, P. W. Thorne, V. F. Banzon, T. Boyer, G. Chepurin, J. H. Lawrimore, M. J. Menne, T. M. Smith, R. S. Vose, H.-M. Zhang, Extended reconstructed sea surface temperature, version 5 (ERSSTv5): Upgrades, validations, and intercomparisons. *J. Clim.* **30**, 8179–8205 (2017).
42. H. M. van Aken, Variability of the water temperature in the western Wadden Sea on tidal to centennial time scales. *J. Sea Res.* **60**, 227–234 (2008).
43. W. de Nooijer, Q. Zhang, Q. Li, Q. Zhang, X. Li, Z. Zhang, C. Guo, K. H. Nisancioglu, A. M. Haywood, J. C. Tindall, S. J. Hunter, H. J. Dowsett, C. Stepanek, G. Lohmann, B. L. Otto-Bliesner, R. Feng, L. E. Sohl, M. A. Chandler, N. Tan, C. Contoux, G. Ramstein, M. L. J. Baatsen, A. S. von der Heydt, D. Chandan, W. R. Peltier, A. Abe-Ouchi, W.-L. Chan, Y. Kamae, C. M. Brierley, Evaluation of Arctic warming in mid-Pliocene climate simulations. *Clim. Past* **16**, 2325–2341 (2020).
44. Z. Song, M. Latif, W. Park, Y. Zhang, Influence of model bias on simulating North Atlantic sea surface temperature during the mid-Pliocene. *Paleocean. Paleoclimatol.* **33**, 884–893 (2018).
45. F. Cook, R. O. Smith, M. Roughan, N. J. Cullen, N. Shears, M. Bowen, Marine heatwaves in shallow coastal ecosystems are coupled with the atmosphere: Insights from half a century of daily in situ temperature records. *Front. Climate* **4**, 1012022 (2022).
46. J. Sharples, O. N. Ross, B. E. Scott, S. P. R. Greenstreet, H. Fraser, Inter-annual variability in the timing of stratification and the spring bloom in the North-western North Sea. *Cont. Shelf Res.* **26**, 733–751 (2006).
47. A. Valentine, A. L. A. Johnson, M. J. Leng, H. J. Sloane, P. S. Balson, Isotopic evidence of cool winter conditions in the mid-Piacenzian (Pliocene) of the southern North Sea Basin. *Palaeogeogr. Palaeoclimatol. Palaeoecol.* **309**, 9–16 (2011).
48. B. C. O'Neill, C. Tebaldi, D. P. van Vuuren, V. Eyring, P. Friedlingstein, G. Hurtt, R. Knutti, E. Kriegler, J.-F. Lamarque, J. Lowe, G. A. Meehl, R. Moss, K. Riahi, B. M. Sanderson, The Scenario Model Intercomparison Project (ScenarioMIP) for CMIP6. *Geosci. Model Dev.* **9**, 3461–3482 (2016).
49. J. E. Tierney, C. J. Poulsen, I. P. Montañez, T. Bhattacharya, R. Feng, H. L. Ford, B. Hönisch, G. N. Inglis, S. V. Petersen, N. Sagoo, C. R. Tabor, K. Thirumalai, J. Zhu, N. J. Burls, G. L. Foster, Y. Goddéris, B. T. Huber, L. C. Ivany, S. K. Turner, D. J. Lunt, J. C. McElwain, B. J. W. Mills, B. L. Otto-Bliesner, A. Ridgwell, Y. G. Zhang, Past climates inform our future. *Science* **370**, eaay3701 (2020).
50. M. P. Byrne, P. A. O'Gorman, Trends in continental temperature and humidity directly linked to ocean warming. *Proc. Natl. Acad. Sci. U.S.A.* **115**, 4863–4868 (2018).
51. C. Clotten, R. Stein, K. Fahl, S. De Schepper, Seasonal sea ice cover during the warm Pliocene: Evidence from the Iceland Sea (ODP Site 907). *Earth Planet. Sci. Lett.* **481**, 61–72 (2018).
52. J. Knies, P. Cabedo-Sanz, S. T. Belt, S. Baranwal, S. Fietz, A. Rosell-Melé, The emergence of modern sea ice cover in the Arctic Ocean. *Nat. Commun.* **5**, 5608 (2014).
53. T. W. N. Haine, T. Martin, The Arctic-Subarctic sea ice system is entering a seasonal regime: Implications for future Arctic amplification. *Sci. Rep.* **7**, 4618 (2017).
54. A. Dai, D. Luo, M. Song, J. Liu, Arctic amplification is caused by sea-ice loss under increasing CO2. *Nat. Commun.* **10**, 121 (2019).
55. J. Kyselý, R. Huth, Changes in atmospheric circulation over Europe detected by objective and subjective methods. *Theor. Appl. Climatol.* **85**, 19–36 (2006).
56. J. Kyselý, Influence of the persistence of circulation patterns on warm and cold temperature anomalies in Europe: Analysis over the 20th century. *Global Planet. Change* **62**, 147–163 (2008).

57. P. A. Stott, N. Christidis, F. E. L. Otto, Y. Sun, J.-P. Vanderlinden, G. J. van Oldenborgh, R. Vautard, H. von Storch, P. Walton, P. Yiou, F. W. Zwiers, Attribution of extreme weather and climate-related events. *WIREs Clim. Change* **7**, 23–41 (2016).
58. B. Schuldt, A. Buras, M. Arend, Y. Vitasse, C. Beierkuhnlein, A. Damm, M. Gharun, T. E. E. Grams, M. Hauck, P. Hajek, H. Hartmann, E. Hiltbrunner, G. Hoch, M. Holloway-Phillips, C. Körner, E. Larysch, T. Lübbe, D. B. Nelson, A. Rammig, A. Rigling, L. Rose, N. K. Ruehr, K. Schumann, F. Weiser, C. Werner, T. Wohlgemuth, C. S. Zang, A. Kahmen, A first assessment of the impact of the extreme 2018 summer drought on Central European forests. *Basic Appl. Ecol.* **45**, 86–103 (2020).
59. E. Steirou, L. Gerlitz, H. Apel, X. Sun, B. Merz, Climate influences on flood probabilities across Europe. *Hydrol. Earth Syst. Sci.* **23**, 1305–1322 (2019).
60. N. A. Kamenos, North Atlantic summers have warmed more than winters since 1353, and the response of marine zooplankton. *Proc. Natl. Acad. Sci. U.S.A.* **107**, 22442–22447 (2010).
61. C. Schär, P. L. Vidale, D. Lüthi, C. Frei, C. Häberli, M. A. Liniger, C. Appenzeller, The role of increasing temperature variability in European summer heatwaves. *Nature* **427**, 332–336 (2004).
62. T. L. Frölicher, E. M. Fischer, N. Gruber, Marine heatwaves under global warming. *Nature* **560**, 360–364 (2018).
63. J. F. Piatt, J. K. Parrish, H. M. Renner, S. K. Schoen, T. T. Jones, M. L. Arimitsu, K. J. Kuletz, B. Bodenstein, M. García-Reyes, R. S. Duerr, R. M. Corcoran, R. S. A. Kaler, G. J. McChesney, R. T. Golightly, H. A. Coletti, R. M. Suryan, H. K. Burgess, J. Lindsey, K. Lindquist, P. M. Warzybok, J. Jahncke, J. Roletto, W. J. Sydeman, Extreme mortality and reproductive failure of common murres resulting from the northeast Pacific marine heatwave of 2014-2016. *PLOS ONE* **15**, e0226087 (2020).
64. T. P. Hughes, J. T. Kerry, M. Álvarez-Noriega, J. G. Álvarez-Romero, K. D. Anderson, A. H. Baird, R. C. Babcock, M. Beger, D. R. Bellwood, R. Berkelmans, T. C. Bridge, I. R. Butler, M. Byrne, N. E. Cantin, S. Comeau, S. R. Connolly, G. S. Cumming, S. J. Dalton, G. Diaz-Pulido, C. M. Eakin, W. F. Figueira, J. P. Gilmour, H. B. Harrison, S. F. Heron, A. S. Hoey, J.-P. A. Hobbs, M. O. Hoogenboom, E. V. Kennedy, C. Kuo, J. M. Lough, R. J. Lowe, G. Liu, M. T. McCulloch, H. A. Malcolm, M. J. McWilliam, J. M. Pandolfi, R. J. Pears, M. S. Pratchett, V. Schoepf, T. Simpson, W. J. Skirving, B. Sommer, G. Torda, D. R. Wachenfeld, B. L. Willis, S. K. Wilson, Global warming and recurrent mass bleaching of corals. *Nature* **543**, 373–377 (2017).
65. Scripps Institution of Oceanography, L. Cavole, A. Demko, R. Diner, A. Giddings, I. Koester, C. Pagniello, M.-L. Paulsen, A. Ramirez-Valdez, S. Schwenck, N. Yen, M. Zill, P. Franks, Biological impacts of the 2013–2015 warm-water anomaly in the Northeast Pacific: Winners, losers, and the future. *Oceanography* **29**, 273–285 (2016).
66. H.-O. Pörtner, D. C. Roberts, M. M. B. Tignor, E. S. Poloczanska, K. Mintenbeck, A. Alegría, M. Craig, S. Langsdorf, S. Löschke, V. Möller, A. Okem, B. Rama, *Climate Change 2022: Impacts, Adaptation and Vulnerability. Contribution of Working Group II to the Sixth Assessment Report of the Intergovernmental Panel on Climate Change* (Cambridge Univ. Press, 2022).
67. N. M. A. Wichern, N. J. de Winter, A. L. A. Johnson, S. Goolaerts, F. Wesselingh, M. F. Hamers, P. Kaskes, P. Claeys, M. Ziegler, The fossil bivalve *Angulus benedeni benedeni*: A potential seasonally resolved stable-isotope-based climate archive to investigate Pliocene temperatures in the southern North Sea basin. *Biogeosciences* **20**, 2317–2345 (2022).
68. B. R. Schöne, J. Fiebig, M. Pfeiffer, R. Gleβ, J. Hickson, A. L. Johnson, W. Dreyer, W. Oschmann, Climate records from a bivalved Methuselah (Arctica islandica, Mollusca; Iceland). *Palaeogeogr. Palaeoclimatol. Palaeoecol.* **228**, 130–148 (2005).
69. A. N. Meckler, M. Ziegler, M. I. Millán, S. F. Breitenbach, S. M. Bernasconi, Long-term performance of the Kiel carbonate device with a new correction scheme for clumped isotope measurements. *Rapid Commun. Mass Spectrom.* **28**, 1705–1715 (2014).
70. I. A. Müller, A. Fernandez, J. Radke, J. van Dijk, D. Bowen, J. Schwieters, S. M. Bernasconi, Carbonate clumped isotope analyses with the long-integration dual-inlet (LIDI) workflow: Scratching at the lower sample weight boundaries. *Rapid Commun. Mass Spectrom.* **31**, 1057–1066 (2017).
71. S. T. Murray, M. M. Arienzo, P. K. Swart, Determining the Δ47 acid fractionation in dolomites. *Geochim. Cosmochim. Acta* **174**, 42–53 (2016).
72. S. M. Bernasconi, I. A. Müller, K. D. Bergmann, S. F. Breitenbach, A. Fernandez, D. A. Hodell, M. Jaggi, A. N. Meckler, I. Millan, M. Ziegler, Reducing uncertainties in carbonate clumped isotope analysis through consistent carbonate-based standardization. *Geochem. Geophys. Geosyst.* **19**, 2895–2914 (2018).
73. I. J. Kocken, I. A. Müller, M. Ziegler, Optimizing the use of carbonate standards to minimize uncertainties in clumped isotope data. *Geochem. Geophys. Geosyst.* **20**, 5565–5577 (2019).
74. W. A. Brand, S. S. Assonov, T. B. Coplen, Correction for the 17O interference in δ(13C) measurements when analyzing CO2 with stable isotope mass spectrometry (IUPAC Technical Report). *Pure Appl. Chem.* **82**, 1719–1733 (2010).
75. N. J. de Winter, ShellChron 0.2.8: A new tool for constructing chronologies in accretionary carbonate archives from stable oxygen isotope profiles. *Geosci. Model Dev.*, 1–37 (2021).
76. N. J. de Winter, T. Agterhuis, M. Ziegler, Optimizing sampling strategies in high-resolution paleoclimate records. *Clim. Past* **17**, 1315–1340 (2021).
77. N. Meinicke, M. A. Reimi, A. C. Ravelo, A. N. Meckler, Coupled Mg/Ca and clumped isotope measurements indicate lack of substantial mixed layer cooling in the Western Pacific Warm Pool During the last ~5 million years. *Paleoceanog. Paleoclimatol.* **36**, e2020Pa004115 (2021).
78. K. W. Huntington, J. M. Eiler, H. P. Affek, W. Guo, M. Bonifacie, L. Y. Yeung, N. Thiagarajan, B. Passey, A. Tripati, M. Daëron, Methods and limitations of 'clumped' CO2 isotope (Δ47) analysis by gas-source isotope ratio mass spectrometry. *J. Mass Spectrom.* **44**, 1318–1329 (2009).
79. M. Iturbide, J. Fernández, J. M. Gutiérrez, A. Pirani, D. Huard, A. Al Khourdajie, J. Baño-Medina, J. Bedia, A. Casanueva, E. Cimadevilla, A. S. Cofiño, M. De Felice, J. Diez-Sierra, M. García-Díez, J. Goldie, D. A. Herrera, S. Herrera, R. Manzanas, J. Milovac, A. Radhakrishnan, D. San-Martín, A. Spinuso, K. M. Thyng, C. Trenham, Ö. Yelekçi, Implementation of FAIR principles in the IPCC: The WGI AR6 Atlas repository. *Sci. Data* **9**, 629 (2022).
80. R Core Team, *R: A Language and Environment for Statistical Computing* (R Foundation for Statistical Computing, 2023); https://R-project.org/.
81. J. Schindelin, I. Arganda-Carreras, E. Frise, V. Kaynig, M. Longair, T. Pietzsch, S. Preibisch, C. Rueden, S. Saalfeld, B. Schmid, Fiji: An open-source platform for biological-image analysis. *Nat. Methods* **9**, 676–682 (2012).
82. H. Dowsett, A. Dolan, D. Rowley, R. Moucha, A. M. Forte, J. X. Mitrovica, M. Pound, U. Salzmann, M. Robinson, M. Chandler, K. Foley, A. Haywood, The PRISM4 (mid-Piacenzian) paleoenvironmental reconstruction. *Clim. Past* **12**, 1519–1538 (2016).
83. L. E. Lisiecki, M. E. Raymo, A Pliocene-Pleistocene stack of 57 globally distributed benthic δ18O records. *Paleoceanography* **20**, PA1003 (2005).
84. J. K. Cochran, K. Kallenberg, N. H. Landman, P. J. Harries, D. Weinreb, K. K. Turekian, A. J. Beck, W. A. Cobban, Effect of diagenesis on the Sr, O, and C isotope composition of late Cretaceous mollusks from the Western Interior Seaway of North America. *Am. J. Sci.* **310**, 69–88 (2010).
85. N. J. de Winter, J. Vellekoop, A. J. Clark, P. Stassen, R. P. Speijer, P. Claeys, The giant marine gastropod Campanile giganteum (Lamarck, 1804) as a high-resolution archive of seasonality in the Eocene greenhouse world. *Geochem. Geophys. Geosyst.* **21**, e2019GC008794 (2020).
86. N. Höche, M. Peharda, E. O. Walliser, B. R. Schöne, Morphological variations of crossed-lamellar ultrastructures of Glycymeris bimaculata (Bivalvia) serve as a marine temperature proxy. *Estuarine Coastal Shelf Sci.* **237**, 106658 (2020).
87. G. Crippa, E. Griesshaber, A. G. Checa, E. M. Harper, M. S. Roda, W. W. Schmahl, Orientation patterns of aragonitic crossed-lamellar, fibrous prismatic and myostracal microstructures of modern Glycymeris shells. *J. Struct. Biol.* **212**, 107653 (2020).
88. K. Janiszewska, M. Mazur, M. Machalski, J. Stolarski, From pristine aragonite to blocky calcite: Exceptional preservation and diagenesis of cephalopod nacre in porous Cretaceous limestones. *PLOS ONE* **13**, e0208598 (2018).
89. V. Barbin, K. Ramseyer, J. P. Debenay, E. Schein, M. Roux, D. Decrouez, Cathodoluminescence of recent biogenic carbonates: Environmental and ontogenetic fingerprint. *Geol. Mag.* **128**, 19–26 (1991).
90. V. Barbin, Cathodoluminescence of carbonate shells: Biochemical vs diagenetic process, in *Cathodoluminescence in Geosciences* (Springer, 2000), pp. 303–329.
91. U. Brand, J. Veizer, Chemical diagenesis of a multicomponent carbonate system–1: Trace elements. *J. Sediment. Res.* **50**, 1219–1236 (1980).
92. N. J. de Winter, P. Claeys, Micro X-ray fluorescence (μXRF) line scanning on Cretaceous rudist bivalves: A new method for reproducible trace element profiles in bivalve calcite. *Sedimentology* **64**, 231–251 (2017).
93. M. Pagel, V. Barbin, P. Blanc, D. Ohnenstetter, *Cathodoluminescence in Geosciences* (Springer Science & Business Media, 2013).
94. T. Götte, D. K. Richter, Quantitative aspects of Mn-activated cathodoluminescence of natural and synthetic aragonite. *Sedimentology* **56**, 483–492 (2009).
95. M. Cusack, Biomineral electron backscatter diffraction for palaeontology. *Palaeontology* **59**, 171–179 (2016).
96. L. A. Casella, E. Griesshaber, X. Yin, A. Ziegler, V. Mavromatis, D. Müller, A.-C. Ritter, D. Hippler, E. M. Harper, M. Dietzel, A. Immenhauser, B. R. Schöne, L. Angiolini, W. W. Schmahl, Experimental diagenesis: Insights into aragonite to calcite transformation of *Arctica islandica* shells by hydrothermal treatment. *Biogeosciences* **14**, 1461–1492 (2017).
97. A.-C. Ritter, V. Mavromatis, M. Dietzel, O. Kwiecien, F. Wiethoff, E. Griesshaber, L. A. Casella, W. W. Schmahl, J. Koelen, R. D. Neuser, A. Leis, D. Buhl, A. Niedermayr, S. F. M. Breitenbach, S. M. Bernasconi, A. Immenhauser, Exploring the impact of diagenesis on (isotope) geochemical and microstructural alteration features in biogenic aragonite. *Sedimentology* **64**, 1354–1380 (2017).
98. M. C. Marcano, T. D. Frank, S. B. Mukasa, K. C. Lohmann, M. Taviani, Diagenetic incorporation of Sr into aragonitic bivalve shells: Implications for chronostratigraphic and palaeoenvironmental interpretations. *Depos. Rec.* **1**, 38–52 (2015).

99. S. V. Popov, Formation of bivalve shells and their microstructure. *Paleontol. J.* **48**, 1519–1531 (2014).
100. A. G. Checa, F. J. Esteban-Delgado, A. B. Rodríguez-Navarro, Crystallographic structure of the foliated calcite of bivalves. *J. Struct. Biol.* **157**, 393–402 (2007).
101. P. S. Freitas, L. J. Clarke, H. Kennedy, C. A. Richardson, Ion microprobe assessment of the heterogeneity of Mg/Ca, Sr/Ca and Mn/Ca ratios in Pecten maximus and Mytilus edulis (bivalvia) shell calcite precipitated at constant temperature. *Biogeosciences* **6**, 1209–1227 (2009).
102. N. de Winter, M. Sinnesael, C. Makarona, S. Vansteenberge, P. Claeys, Trace element analyses of carbonates using portable and micro-X-ray fluorescence: Performance and optimization of measurement parameters and strategies. *J. Anal. At. Spectrom.* **32**, 1211–1223 (2017).
103. J. Vellekoop, P. Kaskes, M. Sinnesael, J. Huygh, T. Déhais, J. W. M. Jagt, R. P. Speijer, P. Claeys, A new age model and chemostratigraphic framework for the Maastrichtian type area (southeastern Netherlands, northeastern Belgium). *Newslett. Stratigr.* **55**, 479–501 (2022).
104. I. S. Al-Aasm, J. Veizer, Diagenetic stabilization of aragonite and low-mg calcite, I. Trace elements in rudists. *J. Sediment. Res.* **56**, 763–770 (1986).
105. J. P. Hendry, P. W. Ditchfield, J. D. Marshall, Two-stage neomorphism of Jurassic aragonitic bivalves: Implications for early diagenesis. *J. Sediment. Res.* **65**, 214–224 (1995).
106. M. Carré, I. Bentaleb, O. Bruguier, E. Ordinola, N. T. Barrett, M. Fontugne, Calcification rate influence on trace element concentrations in aragonitic bivalve shells: Evidences and mechanisms. *Geochim. Cosmochim. Acta* **70**, 4906–4920 (2006).
107. B. Lafuente, R. T. Downs, H. Yang, N. Stone, 1. The power of databases: The RRUFF project, in *Highlights in Mineralogical Crystallography* (De Gruyter (O), 2015), pp. 1–30.
108. P. Ghosh, J. Adkins, H. Affek, B. Balta, W. Guo, E. A. Schauble, D. Schrag, J. M. Eiler, 13C–18O bonds in carbonate minerals: A new kind of paleothermometer. *Geochim. Cosmochim. Acta* **70**, 1439–1456 (2006).
109. M. Daëron, D. Blamart, M. Peral, H. P. Affek, Absolute isotopic abundance ratios and the accuracy of Δ47 measurements. *Chem. Geol.* **442**, 83–96 (2016).
110. IAEA-C-2, Nucleus; https://nucleus.iaea.org/sites/ReferenceMaterials.
111. I. A. Müller, J. D. Rodriguez-Blanco, J.-C. Storck, G. S. D. Nascimento, T. R. R. Bontognali, C. Vasconcelos, L. G. Benning, S. M. Bernasconi, Calibration of the oxygen and clumped isotope thermometers for (proto-)dolomite based on synthetic and natural carbonates. *Chem. Geol.* **525**, 1–17 (2019).
112. S. M. Bernasconi, M. Daëron, K. D. Bergmann, M. Bonifacie, A. N. Meckler, H. P. Affek, N. Anderson, D. Bajnai, E. Barkan, E. Beverly, D. Blamart, L. Burgener, D. Calmels, C. Chaduteau, M. Clog, B. Davidheiser-Kroll, A. Davies, F. Dux, J. Eiler, B. Elliott, A. C. Fetrow, J. Fiebig, S. Goldberg, M. Hermoso, K. W. Huntington, E. Hyland, M. Ingalls, M. Jaggi, C. M. John, A. B. Jost, S. Katz, J. Kelson, T. Kluge, I. J. Kocken, A. Laskar, T. J. Leutert, D. Liang, J. Lucarelli, T. J. Mackey, X. Mangenot, N. Meinicke, S. E. Modestou, I. A. Müller, S. Murray, A. Neary, N. Packard, B. H. Passey, E. Pelletier, S. Petersen, A. Piasecki, A. Schauer, K. E. Snell, P. K. Swart, A. Tripati, D. Upadhyay, T. Vennemann, I. Winkelstern, D. Yarian, N. Yoshida, N. Zhang, M. Ziegler, InterCarb: A community effort to improve interlaboratory standardization of the carbonate clumped isotope thermometer using carbonate standards. *Geochem. Geophys. Geosyst.* **22**, e2020GC009588 (2021).
113. N. de Winter, T. Agterhuis, M. Ziegler, Optimizing sampling strategies in high-resolution paleoclimate records. *Clim. Past Discuss.* **17**, 1315–1340 (2020).
114. D. Chandan, W. R. Peltier, Regional and global climate for the mid-Pliocene using the University of Toronto version of CCSM4 and PlioMIP2 boundary conditions. *Clim. Past* **13**, 919–942 (2017).
115. M. L. J. Baatsen, A. S. von der Heydt, M. A. Kliphuis, A. M. Oldeman, J. E. Weiffenbach, Warm mid-Pliocene conditions without high climate sensitivity: The CCSM4-Utrecht (CESM 1.0.5) contribution to the PlioMIP2. *Clim. Past* **18**, 657–679 (2022).
116. C. Stepanek, E. Samakinwa, G. Knorr, G. Lohmann, Contribution of the coupled atmosphere–ocean–sea ice–vegetation model COSMOS to the PlioMIP2. *Clim. Past* **16**, 2275–2323 (2020).
117. J. Zheng, Q. Zhang, Q. Li, Q. Zhang, M. Cai, Contribution of sea ice albedo and insulation effects to Arctic amplification in the EC-Earth Pliocene simulation. *Clim. Past* **15**, 291–305 (2019).
118. M. Kelley, G. A. Schmidt, L. S. Nazarenko, S. E. Bauer, R. Ruedy, G. L. Russell, A. S. Ackerman, I. Aleinov, M. Bauer, R. Bleck, V. Canuto, G. Cesana, Y. Cheng, T. L. Clune, B. I. Cook, C. A. Cruz, A. D. Del Genio, G. S. Elsaesser, G. Faluvegi, N. Y. Kiang, D. Kim, A. A. Lacis, A. Leboissetier, A. N. LeGrande, K. K. Lo, J. Marshall, E. E. Matthews, S. McDermid, K. Mezuman, R. L. Miller, L. T. Murray, V. Oinas, C. Orbe, C. P. García-Pando, J. P. Perlwitz, M. J. Puma, D. Rind, A. Romanou, D. T. Shindell, S. Sun, N. Tausnev, K. Tsigaridis, G. Tselioudis, E. Weng, J. Wu, M.-S. Yao, GISS-E2.1: Configurations and climatology. *J. Adv. Model. Earth Syst.* **12**, e2019MS002025 (2020).
119. S. J. Hunter, A. M. Haywood, A. M. Dolan, J. C. Tindall, The HadCM3 contribution to PlioMIP phase 2. *Clim. Past* **15**, 1691–1713 (2019).
120. J.-L. Dufresne, M.-A. Foujols, S. Denvil, A. Caubel, O. Marti, O. Aumont, Y. Balkanski, S. Bekki, H. Bellenger, R. Benshila, S. Bony, L. Bopp, P. Braconnot, P. Brockmann, P. Cadule, F. Cheruy, F. Codron, A. Cozic, D. Cugnet, N. de Noblet, J.-P. Duvel, C. Ethé, L. Fairhead, T. Fichefet, S. Flavoni, P. Friedlingstein, J.-Y. Grandpeix, L. Guez, E. Guilyardi, D. Hauglustaine, F. Hourdin, A. Idelkadi, J. Ghattas, S. Joussaume, M. Kageyama, G. Krinner, S. Labetoulle, A. Lahellec, M.-P. Lefebvre, F. Lefevre, C. Levy, Z. X. Li, J. Lloyd, F. Lott, G. Madec, M. Mancip, M. Marchand, S. Masson, Y. Meurdesoif, J. Mignot, I. Musat, S. Parouty, J. Polcher, C. Rio, M. Schulz, D. Swingedouw, S. Szopa, C. Talandier, P. Terray, N. Viovy, N. Vuichard, Climate change projections using the IPSL-CM5 Earth System Model: From CMIP3 to CMIP5. *Clim. Dyn.* **40**, 2123–2165 (2013).
121. W.-L. Chan, A. Abe-Ouchi, Pliocene Model Intercomparison Project (PlioMIP2) simulations using the Model for Interdisciplinary Research on Climate (MIROC4m). *Clim. Past* **16**, 1523–1545 (2020).
122. X. Li, C. Guo, Z. Zhang, O. H. Otterå, R. Zhang, PlioMIP2 simulations with NorESM-L and NorESM1-F. *Clim. Past* **16**, 183–197 (2020).
123. W. S. Cleveland, E. Grosse, W. M. Shyu, Local regression models, in *Statistical Models in S* (Wadsworth & Brooks/Cole, 1992).
124. H. Ridderinkhof, Tidal and residual flows in the western Dutch Wadden Sea II: An analytical model to study the constant flow between connected tidal basins. *Netherl. J. Sea Res.* **22**, 185–198 (1988).
125. H. M. Van Aken, 140 years of daily observations in a tidal inlet (Marsdiep). *ICES Mar. Sci. Symp.* **219**, 359–361 (2003).
126. P. C. T. Van der Hoeven, Observations of surface water temperature and salinity, State Office of Fishery Research (RIVO): 1860–1981. *KNMI Sci. Rep. WR* **82**, 2 (1982).
127. IPCC AR6-WGI Atlas, https://interactive-atlas.ipcc.ch/atlas.
128. IPCC, *Climate Change 2013: The Physical Science Basis: Working Group I Contribution to the Fifth Assessment Report of the Intergovernmental Panel on Climate Change* (Cambridge Univ. Press, 2013).

Acknowledgments: This research would not have been possible without the dedicated laboratory assistance from A. van Dijk, D. Eefting, I. Kocken, and I. Müller in the Utrecht University clumped isotope laboratory. We would like to thank L. Bik (UU), B. Lippens (VUB), and B. Lacet (VU Amsterdam) for their help with sample preparation and M. Zeilmans (UU) for assistance with high-resolution color scans of the shell specimens. We thank T. Bouten (UU) for help with the SEM analyses, M. Hamer (UU) for assistance with EBSD, J. Trabucho Alexandre (UU) and A. van Leeuwen (UU) for assistance with XRD analyses, A. Niemeyer (UU) for help with cathodoluminescence microscopy, and R. Tagle (Bruker Nano GmbH), S. Goderis, and L. Deriemaker (VUB) for their assistance in the AMGC-VUB XRF laboratory. N.J.d.W. thanks L. de Gier (UU), J. Franke (UU), and B. Verhage (UU) for their assistance with sampling, diagenetic screening, and laboratory analysis. This manuscript benefitted from discussions with P. Scussolini (VU Amsterdam). S.G. is grateful to V. Schelfhout, F. Aerts, M. Reyns, R. Sieckelink, and N. Ouifak of "Mobiliteit en Openbare Werken (MOW)" for granting access to the Verrebroekdok (1999–2000), Deurganckdok (2001–2002), and Deurganckdoksluis (2012–2014) construction sites, allowing the collection of the study material. **Funding:** This work was funded through a Marie Curie Individual Fellowship (grant no. H2020-MSCA-IF-2018—UNBIAS, 843011) and Flemish Research Council (FWO) postdoctoral fellowship (grant no. 12ZB220N), both awarded to N.J.d.W. B.G.-H. is supported by an UU-NIOZ collaboration grant. A.L.A.J. is supported by a grant from the Leverhulme Trust (RPG-2021-090). P.K. was supported by the FWO PhD fellowship 11E6621N. P.C. thanks the VUB Strategic Research Program for support, as well as the FWO—Hercules Program for financing the μXRF instrument at AMGC. **Author contributions:** Below is an overview of author contributions according to the CrediT framework: This study was conceptualized by N.J.d.W., P.C., J.T., F.W., and M.Z. Data curation was done by N.J.d.W., F.H., and P.C. Formal analysis was carried out by N.J.d.W., B.M., and S.v.L. Funding for the project was acquired by N.J.d.W., P.C., and M.Z. Investigation and experimental work were done by N.J.d.W., B.G.-H., N.W., P.K., F.H., F.W., and B.M. N.J.d.W., J.T., F.W., P.C., and M.Z. were responsible for the development of the methodology. The project was managed by N.J.d.W. under the supervision of P.C. and M.Z. Resources were provided by S.G., F.W., and P.C. Development of software for formal analysis was by N.J.d.W., J.T., and S.v.L. N.J.d.W., A.L.A.J., S.G., P.C., and M.Z. supervised the project. Validation of the reproducibility of the results was by N.J.d.W., J.T., B.G.-H., P.K., F.H., S.v.L., B.M., S.G., F.W., P.C., and M.Z. Visualization of the results was initiated by N.J.d.W., N.W., B.M., S.G., B.G.-H., A.L.A.J., and J.T. The original draft was written by N.J.d.W., P.B., S.G., and J.T. All authors contributed to reviewing and editing subsequent versions of the manuscript. **Competing interests:** The authors declare that they have no competing interests. **Data and materials availability:** All data needed to evaluate the conclusions in the paper are present in the paper and/or the Supplementary Materials. All data on which this study is based are made available through the open-access database Zenodo: https://doi.org/10.5281/zenodo.8378900.

Submitted 31 October 2023
Accepted 11 April 2024
Published 15 May 2024
10.1126/sciadv.adl6717